

Dissolution and Stability of Arsenate/Phosphate Fluorapatite Solid Solution $[Ca_5(P_xAs_{1-x}O_4)_3F]$ in Aqueous Solution at 25 °C

HUAN DENG^{1,2}, LINGYUN MO^{2,*}, YINIAN ZHU^{2,*}, ZONGQIANG ZHU², HUILI LIU², NA HE² and JIE LIU²

¹College of Light Industry and Food Engineering, Guangxi University, Nanning 530004, Guangxi, P.R. China

²College of Environmental Science and Engineering, Guilin University of Technology, Guilin 541004, Guangxi, P.R. China

*Corresponding authors: Fax: +86 773 5895330; Tel: +86 773 5891059; E-mail: molingyun123@126.com; zhuyinian@163.com

Received: 9 January 2014;

Accepted: 15 April 2014;

Published online: 10 January 2015;

AJC-16611

Arsenate/phosphate fluorapatite solid solutions $[Ca_5(P_xAs_{1-x}O_4)_3F]$ were synthesized and characterized and then their dissolution was studied at pH 2 at 25 °C. During the dissolution, the aqueous pH and Ca^{2+} increased quickly at the early stage and achieved a steady state after 48 h. The aqueous F^- and PO_4^{3-} concentrations increased rapidly and achieved a peak value in 1-3 h and then decreased slowly and showed stable after 200-400 h. With the decreasing mole fraction of $Ca_5(PO_4)_3F$ in the solid, the aqueous pH, Ca^{2+} , F^- and AsO_4^{3-} concentrations increased, while the aqueous PO_4^{3-} concentrations decreased. The F^- anion was found to dissolve preferentially and the release of Ca^{2+} was always more in comparison with the release of PO_4^{3-} and AsO_4^{3-} . The dissolution of the phosphate-rich solids followed the Lippmann *solutus* curve, the dissolution of the arsenate-rich precipitates either followed or slightly overshot the Lippmann *solutus* curve, then approached the solutus curve.

Keywords: Apatite group, Arsenic, Fluorine, Lippmann diagram, Dissolution path.

INTRODUCTION

Apatites form a large family of isomorphous compounds and a well-known representative member of the group is fluorapatite $Ca_5(PO_4)_3F$ (FAP). The existence of several natural minerals containing this component has led to their use in many applications, such as in the manufacture of phosphatic fertilizers and in phosphorus chemistry¹.

The apatites exist as accessory minerals in metamorphic rocks and igneous rocks, in veins and deposits and most commonly occur as chief, impure and fine constituent of bones and teeth. Because of their various substitutions, the apatite group minerals are well-known for the compositional changes. In phosphate ores, pentavalent As(V) is known to partly substitute P(V) in the tetrahedral site in fermorite $[(Ca,Sr)_5(PO_4,AsO_4)_3(F,OH)]$ or to totally substitute it in johnbaumite $[Ca_5(AsO_4)_3OH]$, the arsenate analogue of hydroxyapatite and in svabite $[Ca_5(AsO_4)_3F]$, the fluorarsenate analogue of fluorapatite². It is evident that incomplete progress of such a substitution leads to the formation of a series of solid solution of these isomorphs¹.

Many of apatites occurring in ores have been observed to contain more or less arsenic substituting the phosphorus. Arsenate is isostructural and isoelectronic with phosphate, which may facilitate its anion exchange on apatite. The existing literature

confirms the occurrence of this replacing reaction spread over the entire compositional range and can be used to throw light on its mechanism to arrive at the possibility of removal of incorporated arsenic¹. The removal of arsenic(V) from water and/or wastewater using hydroxyapatite was a complex mechanism that included both co-precipitation between calcium hydrogen arsenate and hydroxyapatite in the aqueous solution and ion exchange between calcium hydrogen arsenate and hydroxyl ion. Recovery of arsenic as precipitate from arsenic-containing wastewaters was studied by hydrothermal mineralization treatment. The precipitate obtained by this treatment was a kind of natural mineral [johnbaumite, $Ca_5(AsO_4)_3OH$], which could be easily reused as resources of arsenic compounds^{3,4}.

Extensive synthesis experiments at ambient temperatures were carried out to evaluate the conditions of formation and the solubilities of many different calcium arsenates^{5,6}. Hydroxyapatite (HAP) and fluorapatite (FAP) are the most stable form of calcium phosphate and exhibit a very low solubility. However, the solubilities of johnbaumite $[Ca_5(AsO_4)_3OH]$ and svabite $[Ca_5(AsO_4)_3F]$ are considerably greater than that of hydroxyapatite and fluorapatite⁵⁻⁹, which suggested that the substitution of phosphate in the arsenate compound could greatly reduce their solubilities⁷⁻⁹.

Fluorapatite, arsenate-phosphate fluorapatite solid solution (AsPFA) and arsenate fluorapatite (AsFAP) have environmental

relevance because they contain potentially toxic As and F in significant quantities and thus, upon dissolution, may release these elements in bioavailable form to ecosystems. No research has been carried out on the dissolution and stability of the FAP-AsFAP solid solution. Consequently, there are insufficient data upon which to assess the true environmental risk of arsenic posed by these minerals. Recent researches on the end members fluorapatite and arsenate fluorapatite indicated that these minerals dissolve non-stoichiometrically at pH 2 and at 25, 35 and 45 °C to yield^{8,9} aqueous Ca^{2+} , F^- and PO_4^{3-} or AsO_4^{3-} . If arsenate-phosphate fluorapatite solid solution $[\text{Ca}_5(\text{P}_x\text{As}_{1-x}\text{O}_4)_3\text{F}]$ dissolved in a similar fashion, great amounts of aqueous arsenic could be released to aqueous environments, which may cause significant environmental harm.

In the present work, the $\text{Ca}_5(\text{P}_x\text{As}_{1-x}\text{O}_4)_3\text{F}$ solid solution (AsPFA) was prepared by a precipitation method. The resulting solid solution particles were characterized by various techniques. This paper reports the results of a preliminary study that monitors the dissolution and release of constituent elements (Ca^{2+} , PO_4^{3-} , AsO_4^{3-} , F^-) from synthetic arsenate-phosphate fluorapatite solid solution by batch dissolution experiments. The solid-solution aqueous-solution (SSAS) reaction paths are also discussed through the constructed Lippmann diagram to assess the potential impact of such solid-solutions on the mobility of arsenic in the environment.

EXPERIMENTAL

Solid preparation and characterization: The experimental details for the synthesis of the solid samples by precipitation were based on the following reaction: $5\text{Ca}^{2+} + 3\text{XO}_4^{3-} + \text{F}^- = \text{Ca}_5(\text{XO}_4)_3\text{F}$. Where X = P(V) or As(V) for the end members and (P + As) for the solid solution.

The $\text{Ca}_5(\text{P}_x\text{As}_{1-x}\text{O}_4)_3\text{F}$ solid solution (AsPFA) was prepared by controlled mixing of a solution of 100 mL 0.5 M $\text{Ca}(\text{NO}_3)_2$ and a solution of 60 mL 0.5 M Na_3PO_4 and Na_3AsO_4 and a solution of 20 mL 0.5 M NaF, so that a Ca/(P + As) molar ratio in the mixed solution was 1.67 (Table-1). Ultrapure water and reagent grade chemicals were used for all experiments. The amounts of Na_3PO_4 and Na_3AsO_4 were changed in individual preparation to obtain synthetic solid samples with different mole fractions of fluorapatite and arsenate fluorapatite. The initial solutions were very slowly mixed in a covered beaker. The mixing solution was kept at 70 °C and stirred by using a stirrer at a moderate rate (100 rpm). After 7 days, the

precipitates were settled. The obtained precipitates were washed thoroughly with ultrapure water and then dried at 110 °C for 24 h⁷.

To determine the composition of the synthetic solid, approximately 10 mg of the precipitate was digested in 20 mL of 1 M HNO_3 solution and diluted to 100 mL with ultrapure water. Calcium and arsenic were analyzed by a atomic absorption spectrometer (AAS, Perkin-Elmer AAnalyst 700). It was analyzed for PO_4^{3-} , F^- , Na^+ and NO_3^- by using an ion chromatography (IC, Metrohm 790) or an UV-visible spectrometer (Perkin-Elmer Lambda 20). All obtained precipitates were characterized by powder X-ray diffraction with a diffractometer (XRD, X'Pert PRO) using $\text{CuK}\alpha$ radiation (40 kV and 40 mA). Crystallographic phase identification of the prepared solids was accomplished via comparing the obtained XRD patterns to the standards from the International Center for Diffraction Data (ICDD), which were card #00-015-0876 for calcium fluoride phosphate and #00-023-0112 calcium fluoride arsenate. The morphology of the precipitate was observed by scanning electron microscopy (SEM, Joel JSM-6380 LV). The Fourier-transform infrared spectra were recorded over the range of 4000-400 cm^{-1} by a spectrophotometer (FT-IR, Nicolet Nexus 470).

Dissolution experiments: 0.5 g of the prepared solid was placed in a series of 250 mL polypropylene bottles and then 150 mL of 0.01 M HNO_3 solution was added into the bottles, which were capped and placed in a water bath (25 °C). Water samples (3 mL) were taken from each polypropylene bottle on 14 times (1, 3, 6 and 12 h, 1, 2, 3, 5, 10, 15, 20, 30, 45 and 60 d). After sampling, the water sample volume was replaced with an equivalent amount of ultrapure water. The water samples were then filtered through 0.20 μm pore diameter membrane filters and stabilized by 0.2 % HNO_3 in 25 mL volumetric flask¹⁰. PO_4^{3-} and F^- were analyzed by an ion chromatography and calcium was analyzed using an atomic absorption spectrometer. After 1440 h dissolution, the solids were sampled from the bottles, washed, dried and characterized by XRD, SEM and FT-IR as described above.

Thermodynamic calculations: Associated with dissolution is an assemblage of solid phases, aqueous solution containing dissolved calcium, phosphate, arsenate and fluoride and a pH value. Assuming equilibrium has been attained, the thermodynamic data can be computed through established theoretical principles⁵. In this work, the calculations were conducted using PHREEQC (Version 2.15) together with the minteq.v4.dat database. The free-format input and the order-independent keyword data blocks facilitate the construction of geochemical models that can simulate a wide variety of aqueous-based scenarios¹¹.

The activities of $\text{Ca}^{2+}_{(\text{aq})}$, $\text{PO}_4^{3-}_{(\text{aq})}$, $\text{AsO}_4^{3-}_{(\text{aq})}$ and $\text{F}^-_{(\text{aq})}$ were firstly calculated by using PHREEQC and then the ion activity products (IAPs) with respect to $\text{Ca}_5(\text{P}_x\text{As}_{1-x}\text{O}_4)_3\text{F}$, $\text{Ca}_5(\text{PO}_4)_3\text{F}$ and $\text{Ca}_5(\text{AsO}_4)_3\text{F}$ were determined according to the mass-action expressions.

RESULTS AND DISCUSSION

Solid characterizations: The composition of the prepared solid solution was the intended composition of $\text{Ca}_5(\text{P}_x\text{As}_{1-x}\text{O}_4)_3\text{F}$.

TABLE-1
SUMMARY OF SYNTHESIS AND COMPOSITION
OF THE $\text{Ca}_5(\text{P}_x\text{As}_{1-x}\text{O}_4)_3\text{F}$ SOLID SOLUTION

Sample No.	Volumes of the precursors (mL)				Solid composition
	0.5 M $\text{Ca}(\text{NO}_3)_2$	0.5 M Na_3PO_4	0.5 M Na_3AsO_4	0.5 M NaF	
AsPFA-1	100	6	54	20	$\text{Ca}_5(\text{P}_{0.10}\text{As}_{0.90}\text{O}_4)_3\text{F}$
AsPFA-2	100	12	48	20	$\text{Ca}_5(\text{P}_{0.20}\text{As}_{0.80}\text{O}_4)_3\text{F}$
AsPFA-3	100	18	42	20	$\text{Ca}_5(\text{P}_{0.31}\text{As}_{0.69}\text{O}_4)_3\text{F}$
AsPFA-4	100	24	36	20	$\text{Ca}_5(\text{P}_{0.41}\text{As}_{0.59}\text{O}_4)_3\text{F}$
AsPFA-5	100	30	30	20	$\text{Ca}_5(\text{P}_{0.52}\text{As}_{0.48}\text{O}_4)_3\text{F}$
AsPFA-6	100	36	24	20	$\text{Ca}_5(\text{P}_{0.61}\text{As}_{0.39}\text{O}_4)_3\text{F}$
AsPFA-7	100	42	18	20	$\text{Ca}_5(\text{P}_{0.71}\text{As}_{0.29}\text{O}_4)_3\text{F}$
AsPFA-8	100	48	12	20	$\text{Ca}_5(\text{P}_{0.80}\text{As}_{0.20}\text{O}_4)_3\text{F}$
AsPFA-9	100	54	6	20	$\text{Ca}_5(\text{P}_{0.91}\text{As}_{0.09}\text{O}_4)_3\text{F}$

The atomic Ca/(As + P) ratio was equal to 1.67 which is a stoichiometric ratio of apatite⁷.

The XRD pattern of the synthetic solids confirmed the formation of the $\text{Ca}_5(\text{P}_x\text{As}_{1-x}\text{O}_4)_3\text{F}$ solid solution, which has the apatite type structure (Fig. 1). Fluorapatite and svabite (arsenate fluorapatite) are the two end members of a structural family series. When subjected to XRD, they produce the same peaks; but the peaks exist at different two-theta values. The incorporation of As(V) in the apatite lattice causes a shift in the "d" spacing⁷. All the solid compounds have showed the formation of an apatitic mineral, which differed only in peak location, absolute intensity and peak width of the diffraction patterns. The tetrahedral covalent radius of AsO_4^{3-} (1.18 Å) is greater than that of PO_4^{3-} (1.10 Å) and the lattice of arsenate fluorapatite can be considered to be less firmly bound than that of fluorapatite¹. The reflection peaks of fluorapatite and arsenate fluorapatite were slightly different from each other.

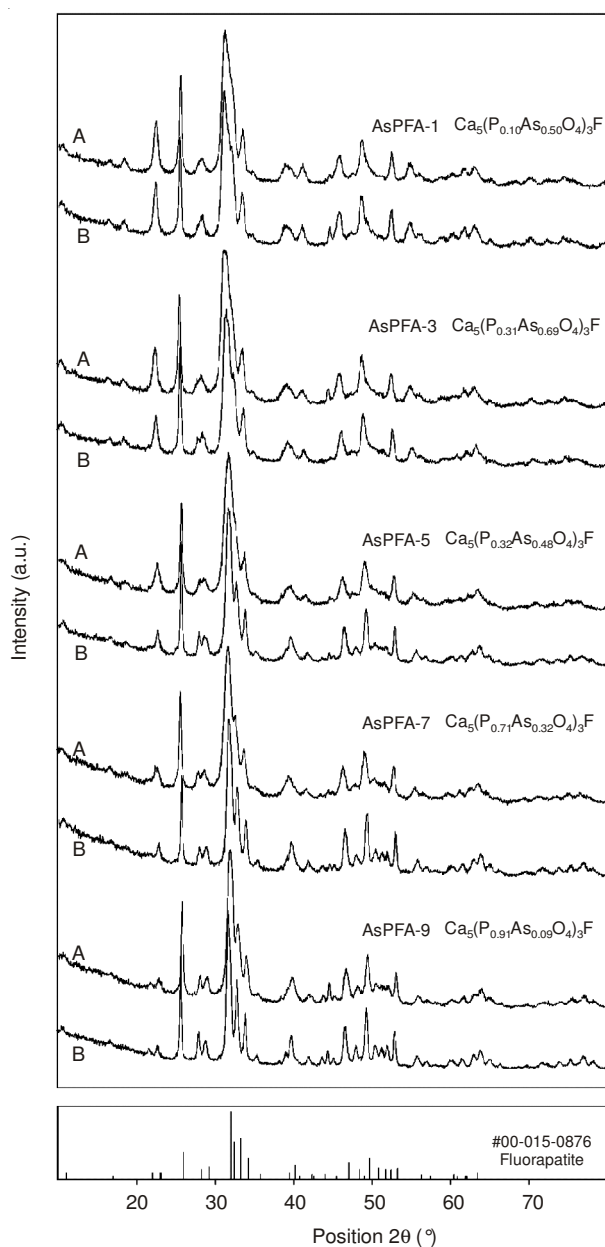


Fig. 1. X-ray diffraction patterns of the apatitic $\text{Ca}_5(\text{P}_x\text{As}_{1-x}\text{O}_4)_3\text{F}$ solid solution before (a) and after (b) dissolution at 25 °C for 120 d

The reflections of the $\text{Ca}_5(\text{P}_x\text{As}_{1-x}\text{O}_4)_3\text{F}$ solid solution shifted gradually to a higher-angle direction when the As/(P + As) molar ratio of the solid samples declined⁷.

The normal FT-IR modes of the tetrahedral phosphate anion are: ν_1 , symmetric P-O stretching; ν_2 , OPO bending; ν_3 , P-O stretching and ν_4 , OPO bending. The FT-IR spectra of the prepared white solids are illustrated in Fig. 2. The fundamental vibrational modes of PO_4^{3-} tetrahedra of apatite phase are noted for all the samples in the region around at 959-965 cm^{-1} (ν_2), 1046-1041, 1095 cm^{-1} (ν_3), 578-566, 606-602 cm^{-1} (ν_4) and 496-491 cm^{-1} (ν_1). The peaks of AsO_4^{3-} appeared around 870-837 cm^{-1} (ν_3) and 430-422, 474-455 cm^{-1} (ν_4). The location of the arsenate peaks and the phosphate peaks in the spectra was witnessed for the whole series of substituted apatites. The area of the phosphate peak was gradually suppressed and the area of the arsenate peak increased as the proportion of arsenate increased⁷.

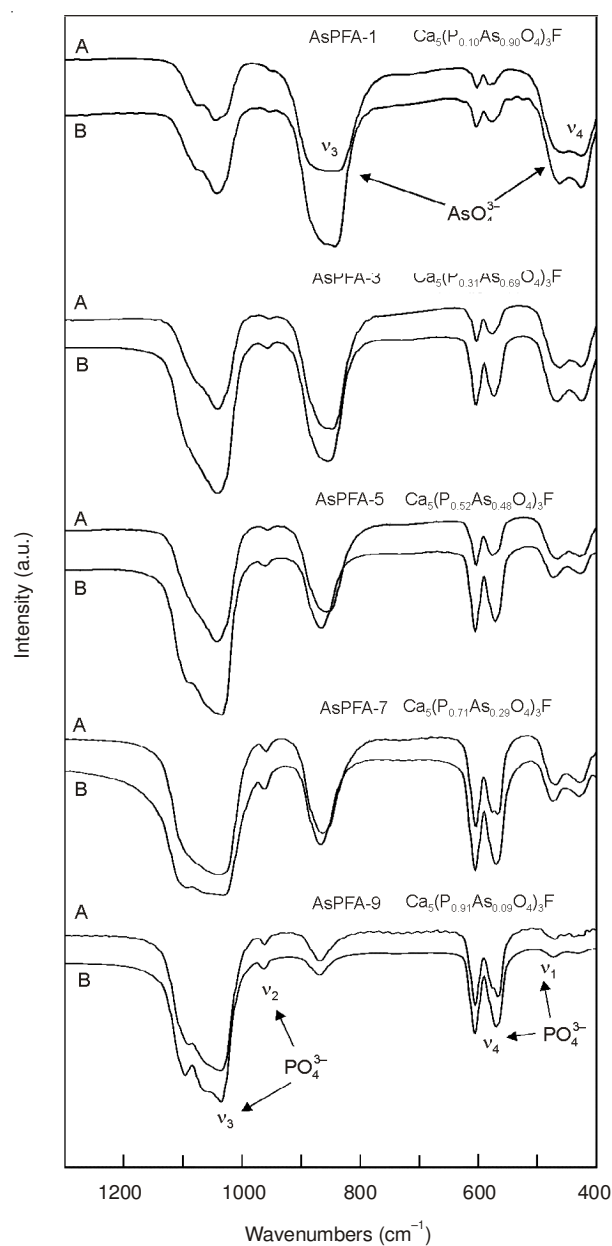


Fig. 2. Infrared spectra of the apatitic $\text{Ca}_5(\text{P}_x\text{As}_{1-x}\text{O}_4)_3\text{F}$ solid solution before (a) and after (b) dissolution at 25 °C for 120 d

As shown in Fig. 3, the scanning electron microscopic observation showed the particle sizes of the solid samples with high As/(P + As) molar ratio of 0.29-1 were $< 1 \mu\text{m}$. However, the difference in crystal shape of apatite was not clear because of the limitation of SEM instrument magnification. The crystal size of the solid samples increases with declining As/(P + As) molar ratio. When the As/(P + As) molar ratio is lower than 0.29, all apatites were large tabular crystals with some particle size $> 5 \mu\text{m}$.

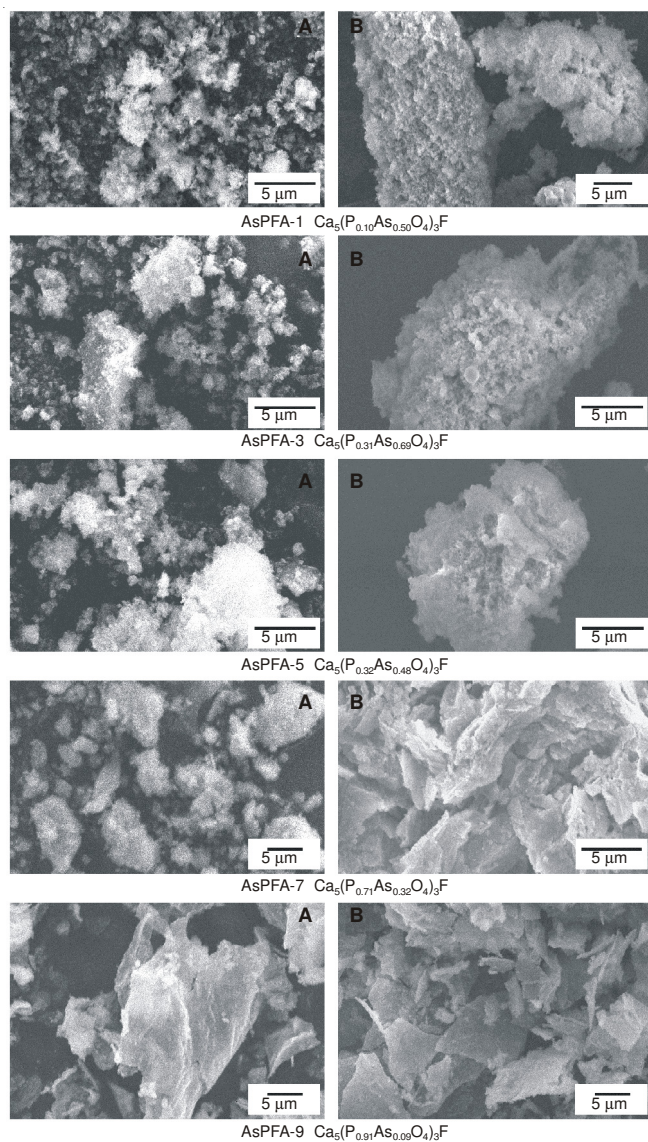


Fig. 3. Scanning electron micrographs of the apatitic $\text{Ca}_5(\text{P}_x\text{As}_{1-x}\text{O}_4)_3\text{F}$ solid solution before (a) and after (b) dissolution at 25°C for 120 d

Solution chemistry: For the apatitic $\text{Ca}_5(\text{P}_x\text{As}_{1-x}\text{O}_4)_3\text{F}$ solid solution, the dissolution occurred primarily within the first 48 h, with dissolution rates declining quickly after this time and steady state conditions achieved, *i.e.*, the pH and the concentrations of Ca^{2+} , PO_4^{3-} , AsO_4^{3-} and F^- in the aqueous solution remained nearly constant over the whole of the experiments (Figs. 4 and 5).

The pH values increased with the increasing dissolution time quickly in the first 48 h and then very slowly or achieved stable until the end of the experiment (Fig. 4). The final pH

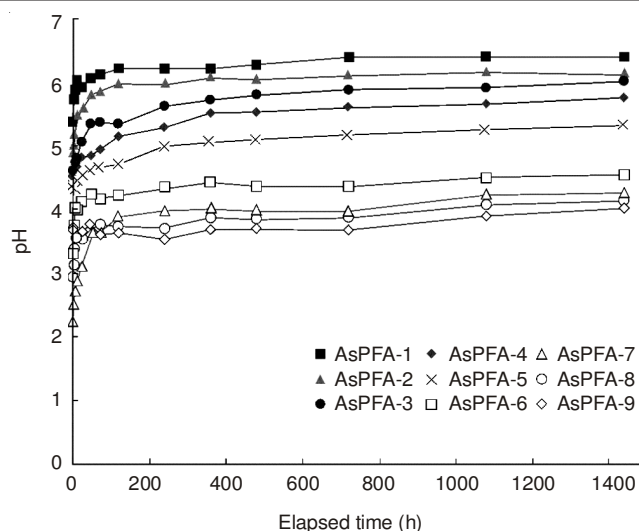


Fig. 4. Aqueous pH versus time for dissolution of the apatitic $\text{Ca}_5(\text{P}_x\text{As}_{1-x}\text{O}_4)_3\text{F}$ solid solution at 25°C

values were strongly related to the mole fraction of fluorapatite in the solid samples. Generally, the pH values increased with the decreasing mole fraction of fluorapatite in the solid, which is possibly the result of the stronger hydrolyzation ability of AsO_4^{3-} than that of PO_4^{3-} .

Similar to the variation of the aqueous pH values, the aqueous Ca^{2+} concentrations increased quickly at the early stage of the dissolution. After reaction for about 48 h, they achieved a plateau. It is also obviously that the aqueous Ca^{2+} concentrations decreased with the increasing mole fraction of fluorapatite in the solid, which could be explained by the higher solubility of the end member $\text{Ca}_5(\text{AsO}_4)_3\text{F}$ than that of the end member $\text{Ca}_5(\text{PO}_4)_3\text{F}$.

The aqueous PO_4^{3-} concentrations increased rapidly at the early stage of the experiment and had achieved a peak value in 1-3 h. After that, the aqueous PO_4^{3-} concentrations declined quickly with time and achieved stable after 50-100 h dissolution. In contrast to the aqueous concentrations of Ca^{2+} , AsO_4^{3-} , F^- and the pH values, the aqueous PO_4^{3-} concentrations increased with the increasing mole fraction of fluorapatite in the solid sample.

The change trend of the aqueous AsO_4^{3-} concentrations with time was considerably influenced by the mole fraction of fluorapatite (Fig. 5). For the solid samples with high mole fraction of fluorapatite (AsPFA-5 - AsPFA-9), the aqueous AsO_4^{3-} concentrations increased with the increasing dissolution time at the beginning of the dissolution experiment. After reaction for about 100-200 h, the concentrations achieved stable. But for the solid samples with low mole fraction of fluorapatite (AsPFA-1 - AsPFA-4), the aqueous AsO_4^{3-} concentrations increased quickly and achieved a peak value in 6-24 h and then declined. After 48 h dissolution, the aqueous AsO_4^{3-} concentrations increased slowly once again and attained stable after 240 h. Generally, the aqueous AsO_4^{3-} concentrations were positively related to the mole fraction of arsenate fluorapatite in the $\text{Ca}_5(\text{P}_x\text{As}_{1-x}\text{O}_4)_3\text{F}$ solid solution, *i.e.*, the AsO_4^{3-} concentrations in the aqueous solution increased with the increasing mole fraction of arsenate fluorapatite in the solid during the solid-solution aqueous-solution (SSAS) reactions. The elemental concentration profiles for F^- are significantly different from

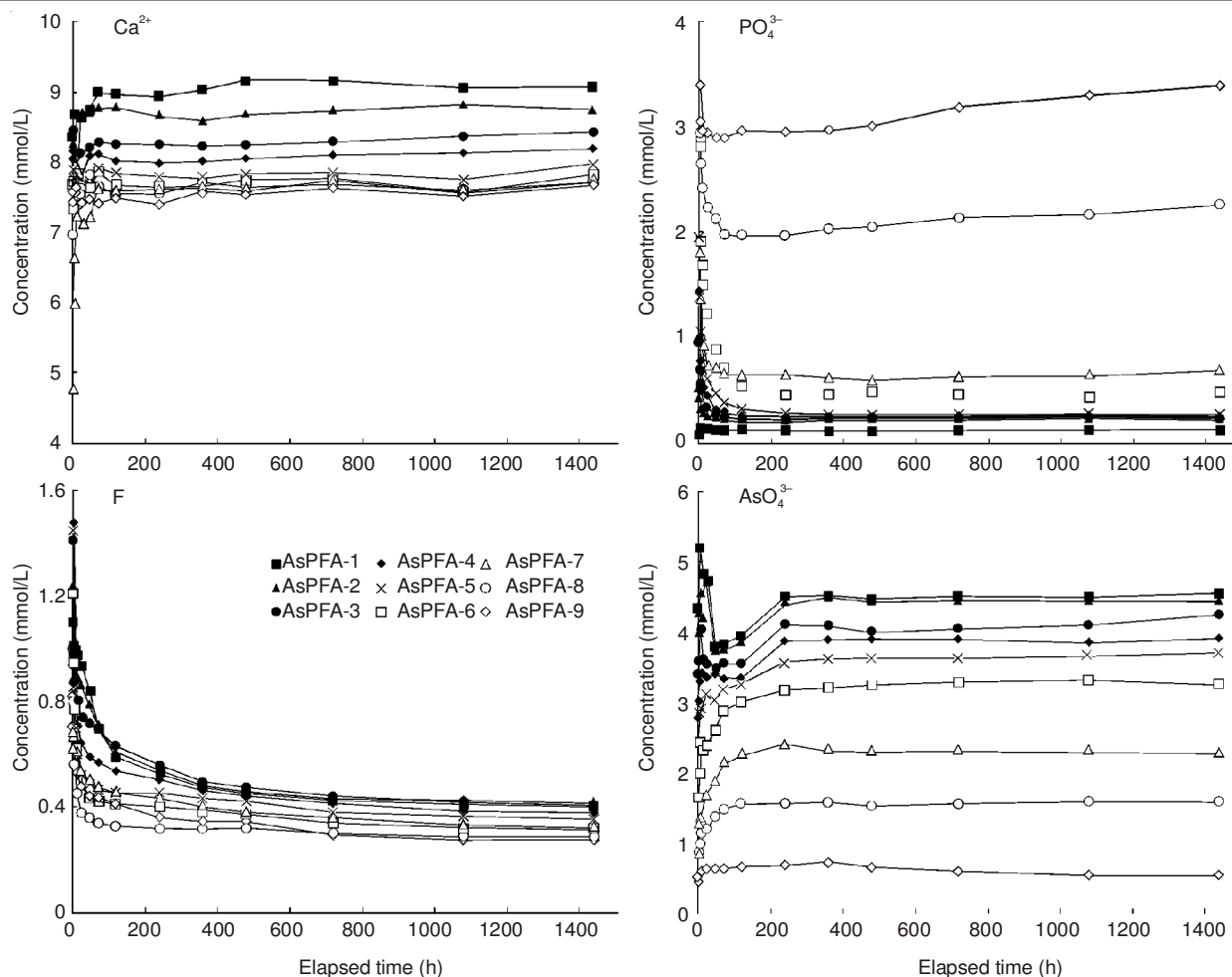


Fig. 5. Aqueous component concentrations versus time for dissolution of the apatitic $\text{Ca}_5(\text{P}_x\text{As}_{1-x}\text{O}_4)_3\text{F}$ solid solution at 25 °C

those for Ca^{2+} in the dissolution (Fig. 5). The aqueous F^- concentrations increased rapidly at the early stage of the experiment and had achieved a peak value in 1 h. Thereafter, the aqueous F^- concentrations declined slowly with time and showed stable after 200–400 h dissolution. Generally, the aqueous F^- concentrations were positively related to the aqueous AsO_4^{3-} concentrations and increased with the increasing mole fraction of arsenate fluorapatite in the solid solution.

It is obviously that the aqueous elements concentrations were strongly depended on the mole fraction of arsenate fluorapatite or the mole fraction of fluorapatite in the $\text{Ca}_5(\text{P}_x\text{As}_{1-x}\text{O}_4)_3\text{F}$ solid solution. Because $\text{Ca}_5(\text{AsO}_4)_3\text{F}$ has a greater solubility than $\text{Ca}_5(\text{PO}_4)_3\text{F}$, the greater the mole fraction of arsenate fluorapatite in the solid solution, the greater the solubility of the solid solution, *i.e.*, the solubility of the $\text{Ca}_5(\text{P}_x\text{As}_{1-x}\text{O}_4)_3\text{F}$ solid solution increased with the increasing mole fractions of arsenate fluorapatite. In the present work, the solubilities or the total milliequivalents of solute per litre of solvent (Σmeq) of the samples increased with an increase in the proportion of arsenate fluorapatite. This could be explained on the basis of the higher dissociation constants of H_3AsO_4 ($K_1 = 4 \times 10^{-3}$, $K_2 = 1 \times 10^{-7}$ and $K_3 = 3.2 \times 10^{-12}$) over the corresponding values of H_3PO_4 ($K_1 = 7.51 \times 10^{-3}$, $K_2 = 6.33 \times 10^{-8}$ and $K_3 = 4.73 \times 10^{-13}$)¹. An additional theoretical substantiation of this experimental finding can be made on the basis of alterations in lattice and solvation energies of ionic crystals brought about by anionic substitution, the rest of the ions being left undisturbed.

The tetrahedral covalent radius of AsO_4^{3-} (1.18 Å) being higher than that of PO_4^{3-} (1.10 Å), the lattice of arsenate fluorapatite can be supposed to be less firmly bound than that of fluorapatite. Solvation energies of the constituent ions of the two lattices being nearly the same, loose packing associated with the lattice of arsenate fluorapatite can account for its greater solubility, which is similar to the dissolution of the solid solution¹. Generally, the aqueous pH and the concentrations of Ca^{2+} , AsO_4^{3-} , F^- in aqueous solution increased simultaneously with the increasing mole fraction of arsenate fluorapatite. On the contrary, the aqueous PO_4^{3-} concentrations decreased with the increasing mole fraction of arsenate fluorapatite or with the decreasing mole fraction of fluorapatite in the solid solution.

Dissolution mechanism

Non-stoichiometry regarding the Ca/(P + As) ratio:

During the dissolution of the $\text{Ca}_5(\text{P}_x\text{As}_{1-x}\text{O}_4)_3\text{F}$ solid solution, the release of calcium into the bulk solution was always more in comparison with the total release of arsenate and phosphate, *i.e.*, the dissolution reaction is non-stoichiometric with calcium being released to solution in stoichiometric excess of arsenate and phosphate (Figs. 4 and 5). When dissolution progressed, release rates of calcium and phosphate quickly increased until the aqueous calcium, arsenate and phosphate concentrations achieved the constant values. And then the over-all rate of the dissolution permanently decreased while the aqueous Ca:(P + As) atomic ratio varied between 1.67 and 2.20.

The transient maximum of the aqueous calcium concentrations during hydroxyapatite dissolution was also observed by previous researchers¹², which was thought to be likely due to a particle size distribution. The smaller the particle size, the greater the solubility and the greater the dissolution rate. Therefore, the greatest value observed in the figure is a consequence of the fast dissolution of the finest particles, with their concurrent greater solubility, followed by re-precipitation to bigger particles which then results in the achievement of the asymptotic solubility value at larger times¹². For the dissolution of the $\text{Ca}_5(\text{P}_x\text{As}_{1-x}\text{O}_4)_3\text{F}$ solid solution in water, after a transient time of 120 h, the aqueous element concentrations and pH values became constant suggesting attainment of a metastable state between the solution and the solid (Figs. 4 and 5).

Accompanying the early release of Ca^{2+} , PO_4^{3-} , AsO_4^{3-} and F^- was a rapid increase in solution pH from 2 to 2.94-5.39 in the first hour of the dissolution and then the solution pH increased very slowly to 4.02-6.41. The proton consumption suggested that adsorption of protons onto negatively charged oxygen ions of phosphate-arsenate groups of the apatitic $\text{Ca}_5(\text{P}_x\text{As}_{1-x}\text{O}_4)_3\text{F}$ solid solution. Sorption of protons results in transformation of surface PO_4^{3-} groups into HPO_4^{2-} or AsO_4^{3-} groups into HAsO_4^{2-} and catalyzes the dissolution process. In addition, the existence of both exchange and dissolution reactions indicates that the protons used up during the dissolution reactions originate not only from sorption-desorption of protons but also from several diverse reactions on the solid surface. An entire explanation of the protons used up during the dissolution must, thus, consider the following reactions, *i.e.*, stoichiometric dissolution of the solid, stoichiometric substitution of 2H^+ for one Ca^{2+} and of one OH^- for one F^- at the solid surface, H^+ adsorption-desorption on the solid surface^{13,14}. These results indicate that the component of the final equilibrated solutions could be controlled by a surface layer of the solid having a component differing from that of the initial $\text{Ca}_5(\text{P}_x\text{As}_{1-x}\text{O}_4)_3\text{F}$ solid solution. The Ca:(P + As) ratios were observed to be 1.67-2.20 in solution in the bottles equilibrated at 25 °C for all solids, which were greater than Ca:P = 1.67 of the $\text{Ca}_5(\text{P}_x\text{As}_{1-x}\text{O}_4)_3\text{F}$ solid solution, which is due to re-precipitation of phosphate and arsenate ions, especially phosphate ions, to the solid surface. Due to the low solubility, the dissolution kinetics was controlled by chemical reactions taking place at the solid surface. The solid is dissolved by ionic detachment of Ca^{2+} and PO_4^{3-} from the solid surface to the aqueous solution. It is proposed that the apatite dissolution in water is constantly non-stoichiometric at atomic level. When an initial part of apatite has been dissolved into the aqueous solution, some amount of Ca^{2+} is returned from the aqueous solution back and adsorbed onto the apatite surface¹⁴.

The saturation indexes were calculated using PHREEQC with respect to calcium phosphates and arsenates that can precipitate in different pH ranges. The results indicated that all aqueous solutions were always undersaturated with respect to calcium phosphates and arsenates, such as $\text{Ca}_8(\text{HPO}_4)_2(\text{PO}_4)_4 \cdot 5\text{H}_2\text{O}$, CaHPO_4 , $\text{CaHPO}_4 \cdot 2\text{H}_2\text{O}$, $\text{Ca}_3(\text{AsO}_4)_2$, $\text{Ca}_3(\text{AsO}_4)_2 \cdot 4\text{H}_2\text{O}$, $\text{Ca}_4(\text{OH})_2(\text{AsO}_4)_2 \cdot 4\text{H}_2\text{O}$, $\text{Ca}(\text{H}_2\text{AsO}_4)_2$, CaHAsO_4 , $\text{Ca}_5(\text{AsO}_4)_3(\text{OH})$, $\text{Ca}_5(\text{AsO}_4)_3\text{F}$ and

portlandite. But the dissolution of the solid solution lead to an increase of supersaturation with respect to $\text{Ca}_5(\text{PO}_4)_3\text{F}$, $\text{Ca}_5(\text{PO}_4)_3(\text{OH})$ and $\text{Ca}_3(\text{PO}_4)_2$. In such a case the dissolution of the solid solution with a Ca/(P + As) ratio of 1.67 would be followed by precipitation of solids with Ca/P ratios of 1.50-1.67. This would lead to a subsequent increase of the Ca/(P + As) ratio in the aqueous solution. The dramatic decay (after the initial rise) in the concentration of phosphate shown in Fig. 5 could be due to the precipitation of minor amounts of calcium phosphate phases with a Ca/P ratio smaller than 1.67.

Non-stoichiometry regarding the Ca/F ratio: Fluoride was released faster than calcium and phosphate/arsenate in comparison with the stoichiometric ratios of the apatitic $\text{Ca}_5(\text{P}_x\text{As}_{1-x}\text{O}_4)_3\text{F}$ solid solution. Apatite dissolution appears to be initiated by the relatively rapid removal from the near surface of F^- . The F^- removal is coupled to phosphate/arsenate hydrolysis. This step was rapid and F^- removal from the fluorapatite surface was complete¹³.

The aqueous Ca:F ratios increased continuously from < 5 to 21.11-28.54 (1440 h). An increase of the Ca/F can be due to the precipitation of a secondary F-bearing phase with the subsequent preferential removal of F^- anions from the aqueous phase. The dramatic decay (after an initial rise) in the concentration of fluorine shown in Fig. 5 can be hardly explained by surface processes. It is most probably a consequence of the precipitation of an F-bearing solid phase. For all aqueous solution samples, the saturation indexes with respect to fluorite were calculated to be 0.11-2.24. At the initial low pH, the dissolution of the solid solution would result in an increase of supersaturation with respect to fluorite. In turn, precipitation of fluorite (CaF_2) would make an increase of the Ca/F ratio in the aqueous solution.

Saturation indexes for fluorapatite and svabite: The thermodynamic analysis could be initiated by assuming the possible pure-phase equilibrium relations¹⁵. Pure-phase equilibrium was assessed by calculating the saturation index (SI), defined by $\text{SI} = \log \text{IAP}/\text{K}_{\text{sp}}$. Where IAP is the ion activity product (*i.e.*, $[\text{Ca}^{2+}]^5[\text{PO}_4^{3-}]^3[\text{F}^-]$ or $[\text{Ca}^{2+}]^5[\text{AsO}_4^{3-}]^3[\text{F}^-]$) and the solubility product K_{sp} is the thermodynamic-equilibrium constant for the dissolution reaction.

Phosphate minerals, especially the apatite-group minerals, are known to be sparingly soluble and fluorapatite is less soluble than arsenate fluorapatite (AsFAP). The K_{sp} value $10^{-55.73}$ for $\text{Ca}_5(\text{PO}_4)_3\text{F}$ given by Zhu *et al.*⁸ was approximately 3.72-3.27 log units lower than 10^{-59} determined by Stumm and Morgan¹⁶. The thermodynamic solubility product for fluorapatite was $\text{K}_{\text{sp}} = 10^{-60.6}$ by Driessens¹⁷. From the result of a batch dissolution for 6 weeks, the $\text{K}_{\text{sp}} = 10^{-70}$ for natural fluorapatite were reported by Valsami-Jones *et al.*¹⁸. A value of K_{sp} for fluorapatite was determined to be $10^{-60.43}$ at 25 °C by Farr and Elmore¹⁹. Inconsistency in literature data could be due to the failure to attain equilibrium, even though some mineral suspensions were equilibrated for as long as 6 weeks or 120 h¹² before being analyzed. Svabite [$\text{Ca}_5(\text{AsO}_4)_3\text{F}$] is a secondary arsenate mineral belonging to the apatite group of phosphates. Its dissolution and subsequent release of aqueous species into aqueous solution play an important role in the cycling of As and F in the environment, but there are few

experimental data on the thermodynamic properties of svabite reported in literature. The mean K_{sp} value was calculated for $Ca_5(AsO_4)_3F$ of $10^{-39.21}$ ($10^{-39.18}$ - $10^{-39.24}$) at 25 °C⁹.

Therefore, the K_{sp} values of $10^{-60.60}$ for fluorapatite and $10^{-39.21}$ for svabite were used in the calculation with PHREEQC. The calculated saturation indexes for svabite show a trend of increasing values as the component of the solid phases approaches that of the pure-phase end member, svabite, thereby indicating that $Ca_5(AsO_4)_3F$ is not the equilibrium phase at low $Ca_5(AsO_4)_3F$ mole fraction (Fig. 6). After 240 h of dissolution, the saturation indexes for svabite showed steady-state behavior and at low $Ca_5(AsO_4)_3F$ mole fractions the SI values were still considerably below the values for pure svabite, showing that pure svabite did not control the AsO_4^{3-} concentration in these samples. This result was consistent with the dissolution of the (Ba,Sr)SO₄ precipitates¹⁵.

The calculated saturation indexes for fluorapatite show a distinctly different trend than those for svabite (Fig. 6). At high $Ca_5(AsO_4)_3F$ mole fraction (> 0.5), the fluorapatite saturated index (SI) values decreased as the $Ca_5(PO_4)_3F$ mole fraction increased and show slight over saturation with respect to pure fluorapatite. At low $Ca_5(AsO_4)_3F$ mole fraction (< 0.5), the aqueous phase was slight undersaturated with respect to pure fluorapatite.

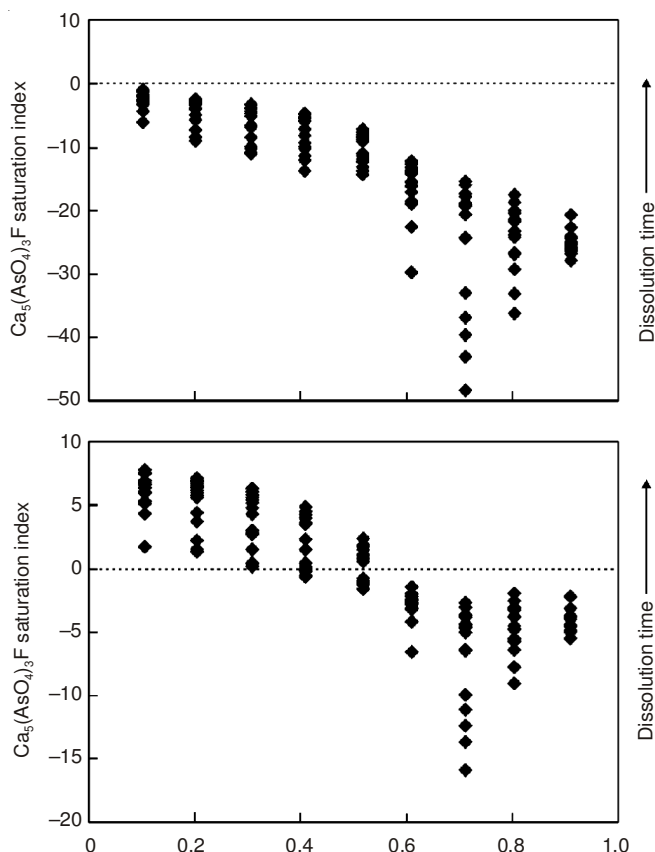
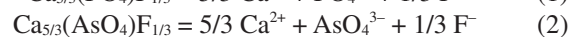
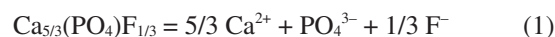


Fig. 6. Saturation indices for fluorapatite [$Ca_5(PO_4)_3F$] and svabite [$Ca_5(AsO_4)_3F$]

Construction of Lippmann diagram: A comprehensive theoretical methodology for describing reaction paths and equilibrium end points in solid-solution aqueous-solution (SSAS) systems had been reported in literatures^{15,20-26}.

When there are several sites per formula unit for the replacing ions, the relationship between the activity of the component and the molar fraction of the replacing ion can be simplified by considering the chemical formula on a "one-substituting-ion" basis. In case of the $Ca_5(P_xAs_{1-x}O_4)_3F$ solid solution, the formula units of the components can be redefined as $Ca_{5/3}(PO_4)F_{1/3}$ and $Ca_{5/3}(AsO_4)F_{1/3}$, which is equivalent to consider the formula unit of the solid solution as $Ca_{5/3}(P_xAs_{1-x}O_4)F_{1/3}$.

The dissolution reactions of the individual components are expressed as



and the mass-action expressions are given by

$$[Ca^{2+}]^{5/3}[PO_4^{3-}][F^-]^{1/3} = K_{Ca_{5/3}(PO_4)F_{1/3}} X_{Ca_{5/3}(PO_4)F_{1/3}} \gamma_{Ca_{5/3}(PO_4)F_{1/3}} \quad (3)$$

$$[Ca^{2+}]^{5/3}[AsO_4^{3-}][F^-]^{1/3} = K_{Ca_{5/3}(AsO_4)F_{1/3}} X_{Ca_{5/3}(AsO_4)F_{1/3}} \gamma_{Ca_{5/3}(AsO_4)F_{1/3}} \quad (4)$$

where designate aqueous activity $K_{Ca_{5/3}(PO_4)F_{1/3}}$ and $K_{Ca_{5/3}(AsO_4)F_{1/3}}$, $X_{Ca_{5/3}(PO_4)F_{1/3}}$ and $X_{Ca_{5/3}(AsO_4)F_{1/3}}$, $\gamma_{Ca_{5/3}(PO_4)F_{1/3}}$ and $\gamma_{Ca_{5/3}(AsO_4)F_{1/3}}$ are the thermodynamic solubility products, the mole fractions (x, 1-x) and the activity coefficients of the $Ca_{5/3}(PO_4)F_{1/3}$ and $Ca_{5/3}(AsO_4)F_{1/3}$ components in the $Ca_{5/3}(P_xAs_{1-x}O_4)F_{1/3}$ solid solution.

Adding eqns. (3) and (4) yields

$$\begin{aligned} \Sigma \Pi_{Ca_{5/3}(P_xAs_{1-x}O_4)F_{1/3}} &= [Ca^{2+}]^{5/3} ([PO_4^{3-}] + [AsO_4^{3-}]) [F^-]^{1/3} \\ &= K_{Ca_{5/3}(PO_4)F_{1/3}} X_{Ca_{5/3}(PO_4)F_{1/3}} \gamma_{Ca_{5/3}(PO_4)F_{1/3}} \\ &\quad + K_{Ca_{5/3}(AsO_4)F_{1/3}} X_{Ca_{5/3}(AsO_4)F_{1/3}} \gamma_{Ca_{5/3}(AsO_4)F_{1/3}} \end{aligned}$$

The term $[Ca^{2+}]^{5/3} ([PO_4^{3-}] + [AsO_4^{3-}]) [F^-]^{1/3}$ is the "total solubility product $\Sigma \Pi_{Ca_{5/3}(P_xAs_{1-x}O_4)F_{1/3}}$ " at equilibrium²³. This relationship, called the *solidus*, defines all possible thermodynamic saturation states for the two-component solid solution series in terms of the solid phase component.

For the problem of a binary solid solution, the activity fractions are defined as

$$X_{PO_4^{3-},(aq)} = \frac{[PO_4^{3-}]}{[PO_4^{3-}] + [AsO_4^{3-}]} \quad (6)$$

$$\text{and } X_{AsO_4^{3-},(aq)} = \frac{[AsO_4^{3-}]}{[PO_4^{3-}] + [AsO_4^{3-}]} \quad (7)$$

Solving eqns. (6) and (7) for $[PO_4^{3-}]$ and $[AsO_4^{3-}]$, respectively and then substituting the results into eqns. (3) and (4) yields

$$\frac{[Ca^{2+}]^{5/3} ([PO_4^{3-}] + [AsO_4^{3-}]) [F^-]^{1/3} X_{PO_4^{3-},(aq)}}{K_{Ca_{5/3}(PO_4)F_{1/3}} \gamma_{Ca_{5/3}(PO_4)F_{1/3}}} = X_{Ca_{5/3}(PO_4)F_{1/3}} \quad (8)$$

$$\frac{[Ca^{2+}]^{5/3} ([PO_4^{3-}] + [AsO_4^{3-}]) [F^-]^{1/3} X_{AsO_4^{3-},(aq)}}{K_{Ca_{5/3}(AsO_4)F_{1/3}} \gamma_{Ca_{5/3}(AsO_4)F_{1/3}}} = X_{Ca_{5/3}(AsO_4)F_{1/3}} \quad (9)$$

Adding eqns.(8) and (9) yields

$$\begin{aligned} & [\text{Ca}^{2+}]^{5/3} ([\text{PO}_4^{3-}] + [\text{AsO}_4^{3-}]) [\text{F}^-]^{1/3} \\ & \left(\frac{X_{\text{PO}_4^{3-}, (\text{aq})}}{K_{\text{Ca}_5/3}(\text{PO}_4)_{\text{F}_{1/3}} \gamma_{\text{Ca}_5/3}(\text{PO}_4)_{\text{F}_{1/3}}} + \frac{X_{\text{AsO}_4^{3-}, (\text{aq})}}{K_{\text{Ca}_5/3}(\text{AsO}_4)_{\text{F}_{1/3}} \gamma_{\text{Ca}_5/3}(\text{AsO}_4)_{\text{F}_{1/3}}} \right) \\ & = X_{\text{Ca}_5/3}(\text{PO}_4)_{\text{F}_{1/3}} + X_{\text{Ca}_5/3}(\text{AsO}_4)_{\text{F}_{1/3}} = 1 \end{aligned} \quad (10)$$

Substituting eqn. (5) into (10) and rearranging yields

$$\Sigma \Pi_{\text{Ca}_5/3}(\text{P}_x\text{As}_{1-x}\text{O}_4)_{\text{F}_{1/3}} = \frac{1}{\frac{X_{\text{PO}_4^{3-}, (\text{aq})}}{K_{\text{Ca}_5/3}(\text{PO}_4)_{\text{F}_{1/3}} \gamma_{\text{Ca}_5/3}(\text{PO}_4)_{\text{F}_{1/3}}} + \frac{X_{\text{AsO}_4^{3-}, (\text{aq})}}{K_{\text{Ca}_5/3}(\text{AsO}_4)_{\text{F}_{1/3}} \gamma_{\text{Ca}_5/3}(\text{AsO}_4)_{\text{F}_{1/3}}}} \quad (11)$$

which is the equation of the *solutus* as given by Glynn and Reardon²³. This relationship defines all possible thermodynamic saturation states for the two-component solid solution series in terms of the aqueous phase composition.

The stoichiometric ion activity product for the $\text{Ca}_5/3(\text{P}_x\text{As}_{1-x}\text{O}_4)_{\text{F}_{1/3}}$ solid solution, IAP_{SS} , is given by

$$\text{IAP}_{\text{SS}} = [\text{Ca}^{2+}]^{5/3} [\text{PO}_4^{3-}]^x [\text{AsO}_4^{3-}]^{(1-x)} [\text{F}^-]^{1/3} \quad (12)$$

Multiplying eqn. (12) by $([\text{PO}_4^{3-}] + [\text{AsO}_4^{3-}])/([\text{PO}_4^{3-}] + [\text{AsO}_4^{3-}])$ and rearranging the terms yields

$$\begin{aligned} \text{IAP}_{\text{SS}} &= [\text{Ca}^{2+}]^{5/3} ([\text{PO}_4^{3-}] + [\text{AsO}_4^{3-}]) [\text{F}^-]^{1/3} \\ \frac{[\text{PO}_4^{3-}]^{x_{\text{Ca}_5/3}(\text{PO}_4)_{\text{F}_{1/3}}}}{([\text{PO}_4^{3-}] + [\text{AsO}_4^{3-}])^{x_{\text{Ca}_5/3}(\text{PO}_4)_{\text{F}_{1/3}}}} &= \frac{[\text{AsO}_4^{3-}]^{x_{\text{Ca}_5/3}(\text{AsO}_4)_{\text{F}_{1/3}}}}{([\text{PO}_4^{3-}] + [\text{AsO}_4^{3-}])^{x_{\text{Ca}_5/3}(\text{AsO}_4)_{\text{F}_{1/3}}}} \end{aligned} \quad (13)$$

or

$$\Sigma \Pi_{\text{SS}} = \frac{\text{IAP}_{\text{SS}}}{\left(X_{\text{PO}_4^{3-}, (\text{aq})} \right)^{x_{\text{Ca}_5/3}(\text{PO}_4)_{\text{F}_{1/3}}} \left(X_{\text{AsO}_4^{3-}, (\text{aq})} \right)^{x_{\text{Ca}_5/3}(\text{AsO}_4)_{\text{F}_{1/3}}}} \quad (14)$$

which is identical to the equation for the solid solution curves given by Glynn and Reardon²³. Substituting eqn. (12) into eqn. (14) and taking the limit as approaches unity yields the end member equation:

$$\begin{aligned} \Sigma \Pi_{\text{Ca}_5/3}(\text{PO}_4)_{\text{F}_{1/3}} &= \frac{[\text{Ca}^{2+}]^{5/3} ([\text{PO}_4^{3-}]) [\text{F}^-]^{1/3}}{\left(X_{\text{PO}_4^{3-}, (\text{aq})} \right)^{x_{\text{Ca}_5/3}(\text{PO}_4)_{\text{F}_{1/3}}}} \\ &= \frac{K_{\text{Ca}_5/3}(\text{PO}_4)_{\text{F}_{1/3}}}{\left(X_{\text{PO}_4^{3-}, (\text{aq})} \right)^{x_{\text{Ca}_5/3}(\text{PO}_4)_{\text{F}_{1/3}}}} \end{aligned} \quad (15)$$

Similarly, $X_{\text{Ca}_5/3}(\text{AsO}_4)_{\text{F}_{1/3}}$ taking the limit as approaches unity yields the end member equation:

$$\begin{aligned} \Sigma \Pi_{\text{Ca}_5/3}(\text{AsO}_4)_{\text{F}_{1/3}} &= \frac{[\text{Ca}^{2+}]^{5/3} ([\text{AsO}_4^{3-}]) [\text{F}^-]^{1/3}}{\left(X_{\text{AsO}_4^{3-}, (\text{aq})} \right)^{x_{\text{Ca}_5/3}(\text{AsO}_4)_{\text{F}_{1/3}}}} \\ &= \frac{K_{\text{Ca}_5/3}(\text{AsO}_4)_{\text{F}_{1/3}}}{\left(X_{\text{AsO}_4^{3-}, (\text{aq})} \right)^{x_{\text{Ca}_5/3}(\text{AsO}_4)_{\text{F}_{1/3}}}} \end{aligned} \quad (16)$$

According to the definition of the total solubility product, the “total solubility product $\Sigma \Pi_{\text{Ca}_5(\text{P}_x\text{As}_{1-x}\text{O}_4)_3\text{F}}$ ” for the formula unit of the solid solution as $\text{Ca}_5(\text{P}_x\text{As}_{1-x}\text{O}_4)_3\text{F}$ can be determined from the “total solubility product $\Sigma \Pi_{\text{Ca}_5/3}(\text{P}_x\text{As}_{1-x}\text{O}_4)_{\text{F}_{1/3}}$ ” by

$$\begin{aligned} \Sigma \Pi_{\text{Ca}_5(\text{P}_x\text{As}_{1-x}\text{O}_4)_3\text{F}} &= [\text{Ca}^{2+}]^5 ([\text{PO}_4^{3-}] + [\text{AsO}_4^{3-}])^3 [\text{F}^-] \\ &= \{ [\text{Ca}^{2+}]^{5/3} ([\text{PO}_4^{3-}] + [\text{AsO}_4^{3-}]) [\text{F}^-]^{1/3} \}^3 = \{ \Sigma \Pi_{\text{Ca}_5/3}(\text{P}_x\text{As}_{1-x}\text{O}_4)_{\text{F}_{1/3}} \}^3 \end{aligned} \quad (17)$$

A Lippmann phase diagram for the solid solution as $\text{Ca}_5(\text{P}_x\text{As}_{1-x}\text{O}_4)_3\text{F}$ is a plot of the solidus and *solutus* as log

$\Sigma \Pi_{\text{Ca}_5(\text{P}_x\text{As}_{1-x}\text{O}_4)_3\text{F}}$ (or $\log \{ \Sigma \Pi_{\text{Ca}_5/3}(\text{P}_x\text{As}_{1-x}\text{O}_4)_{\text{F}_{1/3}} \}^3$) on the ordinate *versus* two superimposed aqueous and solid phase mole fraction scales on the abscissa.

Solid-solution aqueous-solution (SSAS) reaction paths:

This diagram is useful for following SSAS reaction paths²²⁻²³. Dissolution results for the $\text{Ca}_5(\text{P}_x\text{As}_{1-x}\text{O}_4)_3\text{F}$ solid solution at 25 °C are plotted on the Lippmann diagrams in Fig. 7. The

diagrams contain the *solidus* ($\log \Sigma \Pi_{\text{Ca}_5(\text{P}_x\text{As}_{1-x}\text{O}_4)_3\text{F}}$ *vs.* $X_{\text{Ca}_5}(\text{PO}_4)_3\text{F}$)

and the *solutus* ($\log \Sigma \Pi_{\text{Ca}_5(\text{P}_x\text{As}_{1-x}\text{O}_4)_3\text{F}}$ *vs.* $X_{\text{PO}_4^{3-}, (\text{aq})}$) for the

$\text{Ca}_5(\text{P}_x\text{As}_{1-x}\text{O}_4)_3\text{F}$ solid solution series and the total solubility product curves at stoichiometric saturation for the nine solid

solution compositions ($\Sigma \Pi_{\text{SS}}$ *vs.* $X_{\text{PO}_4^{3-}, (\text{aq})}$). Also included are

the data from our study, plotted as $[\text{Ca}^{2+}]^5 ([\text{PO}_4^{3-}] + [\text{AsO}_4^{3-}])^3 [\text{F}^-]$

vs. $X_{\text{PO}_4^{3-}, (\text{aq})}$. Diagrams were constructed by using thermo-

dynamic solubility products for $\text{Ca}_5(\text{PO}_4)_3\text{F}$ of $10^{-60.60}$ and $\text{Ca}_5(\text{AsO}_4)_3\text{F}$ of $10^{-39.21}$ reported by the previous researchers^{8,9,17}.

In these calculations, an idea solid solution was assumed. A similar assumption was also made by Glynn *et al.*²² and Felmy *et al.*¹⁵.

A Lippmann diagram for the $\text{Ca}_5(\text{P}_x\text{As}_{1-x}\text{O}_4)_3\text{F}$ solid solution as the ideal case (Guggenheim coefficient $a_0 = 0.0$) is shown in Fig. 7. The main purpose of the present work is to get some information about the aqueous evolution in contact with the $\text{Ca}_5(\text{P}_x\text{As}_{1-x}\text{O}_4)_3\text{F}$ solid solution and its effect on As and P distribution in water environment. The $\text{Ca}_5(\text{P}_x\text{As}_{1-x}\text{O}_4)_3\text{F}$ solid solution was treated as an ideal case in the construction of Lippmann diagram, since the position of the Lippmann *solutus* curve is insensitive to the excess thermodynamic mixing properties of the solid solutions²². Increasing the excess free energy of the solid solution does not perceptibly vary the position of the Lippmann *solutus*. Only the solidus curve is influenced, indicating a greater degree of partitioning between the solid and aqueous solutions, which has been found in all SSAS systems with great differences in end member solubility products. The larger the difference in solubility products of two end members, the smaller the influence of the thermodynamic mixing properties on the *solutus* position²³. Lippmann diagrams resulting from the application of variable solid phase activity coefficients are rather similar to the one depicting ideal solid solution. The only difference is a slight upward convexity of the solidus. This similarity is owing to the large difference

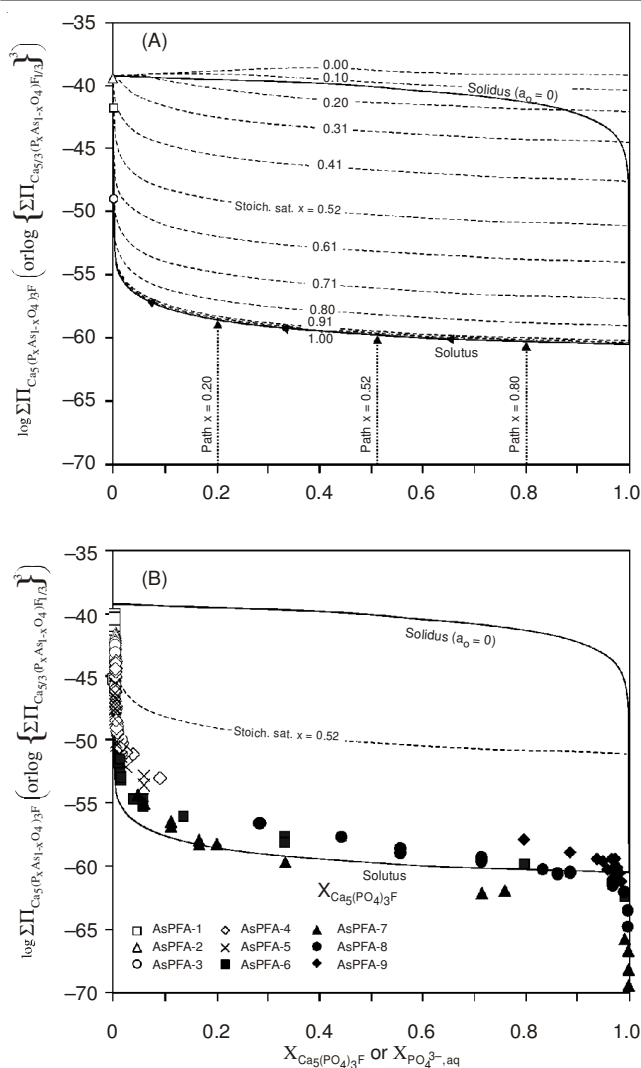


Fig. 7. Lippmann diagrams for dissolution of the $Ca_5(P_xAs_{1-x}O_4)_3F$ solid solution; (a) Hypothetical partial-equilibrium reaction paths for the dissolution of three solid phases $Ca_5(P_xAs_{1-x}O_4)_3F$ ($x = 0.20, 0.52$ and 0.80) are drawn in short-dashed and arrowed lines. Solid arrows show primary saturation states. The triangle, square and circle symbols represent equilibrium end-points for the three solid phases respectively. Long-dashed curves depict the series of possible stoichiometric saturation states for the $Ca_5(P_xAs_{1-x}O_4)_3F$ solid solution; (b) Dissolution results for the $Ca_5(P_xAs_{1-x}O_4)_3F$ solid solution are plotted on the Lippmann diagram

of the solubility products of the two end members²⁷. It could be believed that the behaviour of the SSAS for the $Ca_5(P_xAs_{1-x}O_4)_3F$ solid solution is not seriously influenced by non-ideality in the solid solution.

In a system with great difference in end member solubility products, the curve for the least-soluble end member will closely follow the *solutus* curve, except at aqueous activity-fractions close to the more soluble end member²². In Fig. 7, the saturation curves for the $Ca_5(P_{0.91}As_{0.09}O_4)_3F$ solid solution and the pure $Ca_5(PO_4)_3F$ solid cannot be distinguished from the *solutus*. The great difference between the solubility products of the two end members results in a strong preferential partitioning of the less soluble end member towards the solid phase²⁵, which explains the extremely PO_4^{3-} -poor and AsO_4^{3-} -rich composition of the aqueous solution at the end of the experiment. Lippmann diagrams can be used to describe the

co-existing components of solid and aqueous solution under equilibrium conditions. According to the Lippmann diagram, arsenate fluorapatite-poor solid solution is in equilibrium with AsO_4^{3-} -rich aqueous solution. As a result, from the point of view of the equilibrium thermodynamics, in solidification-stabilization of arsenic-containing hazardous wastes and arsenic-contaminated soil using apatite, large amount of apatite must be used in the process to avoid the leaching of arsenic.

As $Ca_5(P_xAs_{1-x}O_4)_3F$ dissolves in solution with $pH < 7$, aqueous P(V) and As(V) are converted primarily into HPO_4^{2-} and $HAAsO_4^{2-}$ and only a small fractions remain as PO_4^{3-} and AsO_4^{3-} . The small values of the activity fractions are a consequence of the P(V) and As(V) speciation and the fractions of total P(V) and As(V) would be orders of magnitude greater. The Lippmann diagram illustrates that if the rate of dissolution of the original $Ca_5(P_xAs_{1-x}O_4)_3F$ solid solution is slower than the rate of precipitation of secondary phases, the solid precipitated at primary saturation will be a nearly pure $Ca_5(PO_4)_3F$.

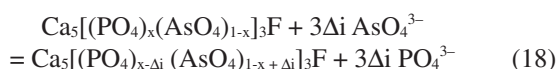
The key problem with using the total solubility product to demonstrate solid-solution aqueous-solution reactions for $Ca_5(P_xAs_{1-x}O_4)_3F$ is clearly show that dissolution is non-stoichiometric. The Lippmann diagram is useful nonetheless if we superimpose stoichiometric saturation curves for each of the solids used in the present work on the Lippmann diagram. Additionally, the minimum stoichiometric saturation curve, *i.e.*, the curve connecting the minimum values of each of the stoichiometric saturation curves, is also plotted in Fig. 7. It can easily be seen in the Lippmann diagram (Fig. 7) that these data plot along the *solutus* curve. Nevertheless, they are not at the appropriate thermodynamic equilibrium points. The data could indicate that the solutions were at primary saturation points suggesting the formation of a secondary phase. However, the data plot in an area where the stoichiometric saturation curves converge toward the *solutus* and the data do plot near to the *solutus* curves. Generally, the position of data points on a Lippmann diagram is related to the aqueous speciation, degree to which secondary phases are formed and the relative rates of dissolution and precipitation²⁰.

An interesting application of the Lippmann diagram (Fig. 7) is the possibility of calculating the component of the solid phase that is in contact with an aqueous solution that is at stoichiometric saturation with respect to the solid phase²⁰. If there is sufficient information to determine ionic activities, then $X_{PO_4^{3-},(aq)}$ can be calculated and the IAP_{SS} determined

using eqn. (12). The value of $X_{Ca_5(PO_4)_3F}$ can be determined using an appropriate numerical method such as Newton iteration. Convergence should be achieved in < 5 iterations even when the initial guess is far from the actual value²⁰. The feasibility of making such calculations is suggested in Fig. 7. The stoichiometric saturation curves are subparallel and the values of $X_{Ca_5(PO_4)_3F}$ are unique for a given $X_{PO_4^{3-},(aq)}$ and $\Sigma \Pi_{SS}$.

There are two potentially essential limiting reaction paths¹⁵. The first path includes stoichiometric dissolution of the solid precipitates up to the first point of saturation (primary saturation) with respect to a secondary solid phase, either a pure solid phase or solid-solution phase, followed by a possible

non-stoichiometric dissolution of the solid precipitates in which an increment of exchange ($3\Delta i$) occurs^{15,22}. For the $\text{Ca}_5(\text{P}_x\text{As}_{1-x}\text{O}_4)_3\text{F}$ solid solution such an exchange reaction could be



In which the solid phases become enriched in the more soluble end member. Such a dissolution pathway should go after the Lippmann *solutus* curve which represents a series of primary saturation states. Non-stoichiometric dissolution will result in the solid phase to become progressively more enriched in the insoluble composition (FAP, PO_4^{3-}), while the aqueous component will shift towards the more soluble end member (arsenate fluorapatite, AsO_4^{3-}) as equilibrium is approached²².

The second dissolution pathway is a stoichiometric dissolution pathway in which the component of the solid phase remains invariant during the dissolution, but the activity ratios in the aqueous phase vary as a function of the reaction progress.

The experimental data plotted on Lippmann phase diagrams indicate that the FAP-rich precipitates ($X_{\text{Ca}_5(\text{PO}_4)_3\text{F}} > 0.5$) follow the Lippmann *solutus* curve, the arsenate fluorapatite-rich precipitates ($X_{\text{Ca}_5(\text{AsO}_4)_3\text{F}} > 0.5$) either follow or slightly overshoot the Lippmann *solutus* curve, then approach the *solutus* curve, showing the dissolution path for these precipitates may involve stoichiometric dissolution to the Lippmann *solutus* curve followed by a possible exchange reaction such as eqn. (18).

The region of stoichiometric dissolution was over before the first samples were taken at 1 h. Our dissolution experimental data show a persistent enrichment in the fluorapatite composition in the solid phase and a persistent enrichment in the AsO_4^{3-} composition in the aqueous phase. The possibility of formation of a phase close in component to pure fluorapatite seems unavoidable, given the extremely low solubility of fluorapatite and the large oversaturation with respect to fluorapatite seen in Fig. 7 for the precipitates with ($X_{\text{Ca}_5(\text{AsO}_4)_3\text{F}} > 0.5$).

For comparison with the Lippmann *solutus* curve, hypothetical stoichiometric saturation curves for the $\text{Ca}_5(\text{P}_x\text{As}_{1-x}\text{O}_4)_3\text{F}$ solids ($x = 0, 0.10, 0.20, \dots, 0.90, 1$) are also plotted on in Fig. 7. The shapes of the stoichiometric saturation curves are similar to the Lippmann *solutus* and closely approximate the *solutus* curve as solid-compositions approach the less soluble end member²².

Several hypothetical reaction paths are illustrated in Fig. 7, in relation to Lippmann *solutus* and solidus curves for the $\text{Ca}_5(\text{P}_x\text{As}_{1-x}\text{O}_4)_3\text{F}$ solid solution. The reaction path of a stoichiometrically dissolving solid solution moves vertically from the *abscissa* of a Lippmann diagram, originating at the mole fraction corresponding to the initial solid solution component. The pathways indicate an initial stoichiometric dissolution up to the *solutus* curve, followed by non-stoichiometric dissolution along the *solutus*, towards the more soluble end member²². Paths A, B and C in Fig. 7 demonstrate hypothetical reaction paths for the solid solution $\text{Ca}_5(\text{P}_{0.20}\text{As}_{0.80}\text{O}_4)_3\text{F}$, $\text{Ca}_5(\text{P}_{0.52}\text{As}_{0.48}\text{O}_4)_3\text{F}$ and $\text{Ca}_5(\text{P}_{0.80}\text{As}_{0.20}\text{O}_4)_3\text{F}$, respectively. The

effects of aqueous speciation of PO_4^{3-} and AsO_4^{3-} on the dissolution were not considered. If one of the replacing anions in the solid-solution undergoes speciation, the stoichiometric dissolution paths move from the activity-fraction lines. However, the end-points are the same to that in the case of no speciation²².

Conclusion

During the dissolution of the synthetic $\text{Ca}_5(\text{P}_x\text{As}_{1-x}\text{O}_4)_3\text{F}$ solid solution at 25 °C and initial pH=2, the aqueous Ca^{2+} , PO_4^{3-} , AsO_4^{3-} and F^- concentration profiles showed a fast initial release of constituent ions to solution followed by a decreasing rate of dissolution and eventually, steady state. The aqueous pH values and Ca^{2+} concentrations increased quickly at the early stage of the dissolution and achieved a metastable state after 48 h. The aqueous F^- and PO_4^{3-} concentrations increased very rapidly at the early stage of the experiment and achieved a peak value in 1-3 h and then decreased slowly with time and showed stable after 200-400 h dissolution. The aqueous element concentrations were considerably influenced by the mole fraction of fluorapatite in the $\text{Ca}_5(\text{P}_x\text{As}_{1-x}\text{O}_4)_3\text{F}$ solid solution. With the decreasing mole fraction of fluorapatite in the solid solution, the aqueous pH values and the aqueous Ca^{2+} , F^- and AsO_4^{3-} concentrations increased, while the aqueous PO_4^{3-} concentrations decreased.

The dissolution of the $\text{Ca}_5(\text{P}_x\text{As}_{1-x}\text{O}_4)_3\text{F}$ solid solution into an initially dilute aqueous solution was often stoichiometric and followed by the non-stoichiometric dissolution. During the non-stoichiometric dissolution, the aqueous PO_4^{3-} concentration decreased and the aqueous AsO_4^{3-} concentration increased. The F^- anion was found to be released preferentially in comparison with calcium, arsenate and phosphate. The release of calcium into the bulk solution was always more in comparison with the total release of arsenate and phosphate.

The solid solution-aqueous solution (SSAS) reaction paths for the dissolution of the synthetic $\text{Ca}_5(\text{P}_x\text{As}_{1-x}\text{O}_4)_3\text{F}$ solid solution were plotted on Lippmann diagrams. Solid phase activity coefficients used in the construction of the Lippmann diagrams were determined with the Guggenheim coefficient of $a_0 = 0$ for an ideal solid solution. Either for the low fluorapatite mole fractions or for the high fluorapatite mole fractions, the dissolution followed or nearly followed the limiting reaction path model as defined by the Lippmann *solutus* curves.

ACKNOWLEDGEMENTS

The authors thank the Guangxi Key Laboratory of Environmental Pollution Control Theory and Technology for the experimental support and the financial assistances from the National Natural Science Foundation of China (NSFC41263009, NSFC40773059), the Provincial Natural Science Foundation of Guangxi (2012GXNSFDA053022, 2011GXNSFF018003) and the Guangxi Science and Technology Development Project (GuiKeZhong1298002-3).

REFERENCES

1. T.S.B. Narasaraaju and D.E. Phebe, *J. Mater. Sci.*, **31**, 1 (1996).
2. M. Kucharski, W. Mroz, J. Kowalczyk, B. Szafirska and M. Gluzinska, *Arch. Metall.*, **47**, 119 (2002).
3. T. Itakura, R. Sasai and H. Itoh, *J. Hazard. Mater.*, **146**, 328 (2007).

4. P.A. O'Day, *Elements*, **2**, 77 (2006).
5. J.V. Bothe Jr. and P.W. Brown, *J. Hazard. Mater.*, **69**, 197 (1999).
6. T. Nishimura and R.G. Robins, *Miner. Process. Extr. Metallur. Rev.*, **18**, 283 (1998).
7. Y. Zhu, Y. Chen, F. Long, J. Lan, N. He and M. Qian, *Metall. Mater. Trans., A Phys. Metall. Mater. Sci.*, **40**, 2659 (2009).
8. Y. Zhu, X. Zhang, Y. Chen, Q. Xie, J. Lan, M. Qian and N. He, *Chem. Geol.*, **268**, 89 (2009).
9. Y. Zhu, X. Zhang, H. Zeng, H. Liu, N. He and M. Qian, *Environ. Chem. Lett.*, **9**, 339 (2011).
10. US Environmental Protection Agency, Trace Elements in Water, Solids and Biosolids by Stabilized Temperature Graphite Furnace Atomic Absorption Spectrometry, US EPA Method 200.9, EPA-821-R-01-011, Washington DC, USA (2001).
11. D.L. Parkhurst and C.A.J. Appelo, Description of Input and Examples for PHREEQC Version 3-A Computer Program for Speciation, Batch-reaction, One-dimensional Transport and Inverse Geochemical Calculations, Geological Survey Techniques and Methods, Book 6, Chap. A43 (1999).
12. M.T. Fulmer, I.C. Ison, C.R. Hankermayer, B.R. Constantz and J. Ross, *Biomaterials*, **23**, 751 (2002).
13. C. Chairat, E.H. Oelkers, J. Schott and J.E. Lartigue, *Geochim. Cosmochim. Acta*, **71**, 5888 (2007).
14. S.V. Dorozhkin, *Prog. Cryst. Growth Charact. Mater.*, **44**, 45 (2002).
15. A.R. Felmy, D. Rai and D.A. Moore, *Geochim. Cosmochim. Acta*, **57**, 4345 (1993).
16. W. Stumm and J.J. Morgan, *Aquatic Chemistry, Chemical Equilibria and Rates in Natural Waters*, John Wiley & Sons Inc., New York (1996).
17. F.C.M. Driessens, *Mineral Aspects of Dentistry*, S. Karger AG, Basel (1982).
18. E. Valsami-Jones, K.W. Ragnarsdottir, A. Putnis, D. Bosbach, A.J. Kemp and G. Cressey, *Chem. Geol.*, **151**, 215 (1998).
19. T.D. Farr and K.L. Elmore, *J. Phys. Chem.*, **66**, 315 (1962).
20. D. Baron and C.D. Palmer, *Geochim. Cosmochim. Acta*, **66**, 2841 (2002).
21. H. Gamsjäger, E. Königsberger and W. Preis, *Aquat. Geochem.*, **6**, 119 (2000).
22. P.D. Glynn, E.J. Reardon, L.N. Plummer and E. Busenberg, *Geochim. Cosmochim. Acta*, **54**, 267 (1990).
23. P.D. Glynn and E.J. Reardon, *Am. J. Sci.*, **290**, 164 (1990).
24. C. Monnin, *Chem. Geol.*, **153**, 187 (1999).
25. M. Prieto, A. Fernández-González, U. Becker and A. Putnis, *Aquat. Geochem.*, **6**, 133 (2000).
26. X. Zhang, Y. Zhu, H. Zeng, D. Wang, J. Liu, H. Liu, M. Qian and L. Xu, *Environ. Chem.*, **8**, 133 (2011).
27. M. Prieto, *Rev. Mineral. Geochem.*, **70**, 47 (2009).